



Co-occurring ripple oscillations facilitate neuronal interactions between cortical locations in humans

Ilya A. Verzhbinsky^{a,b,1} , Daniel B. Rubin^c, Sophie Kajfez^d , Yiting Bu^e, Jessica N. Kelemen^c, Anastasia Kapitonava^c, Ziv M. Williams^f, Leigh R. Hochberg^{c,g,h}, Sydney S. Cash^{c,2} , and Eric Halgren^{d,e,1,2}

Edited by György Buzsáki, New York University Grossman School of Medicine, New York, NY; received July 20, 2023; accepted November 5, 2023

How the human cortex integrates (“binds”) information encoded by spatially distributed neurons remains largely unknown. One hypothesis suggests that synchronous bursts of high-frequency oscillations (“ripples”) contribute to binding by facilitating integration of neuronal firing across different cortical locations. While studies have demonstrated that ripples modulate local activity in the cortex, it is not known whether their co-occurrence coordinates neural firing across larger distances. We tested this hypothesis using local field-potentials and single-unit firing from four 96-channel microelectrode arrays in the supragranular cortex of 3 patients. Neurons in co-rippling locations showed increased short-latency co-firing, prediction of each other’s firing, and co-participation in neural assemblies. Effects were similar for putative pyramidal and interneurons, during non-rapid eye movement sleep and waking, in temporal and Rolandic cortices, and at distances up to 16 mm (the longest tested). Increased co-prediction during co-ripples was maintained when firing-rate changes were equated, indicating that it was not secondary to non-oscillatory activation. Co-rippling enhanced prediction was strongly modulated by ripple phase, supporting the most common posited mechanism for binding-by-synchrony. Co-ripple enhanced prediction is reciprocal, synergistic with local upstates, and further enhanced when multiple sites co-ripple, supporting re-entrant facilitation. Together, these results support the hypothesis that trans-cortical co-occurring ripples increase the integration of neuronal firing of neurons in different cortical locations and do so in part through phase-modulation rather than unstructured activation.

ripples | cortex | human | single neuron | binding

The “binding problem” describes a fundamental question in systems neuroscience: How are the different elements of a mental event unified into a cohesive experience despite being encoded in locations distributed across the cortex? The mechanisms supporting cortical binding are poorly understood, but one proposed mechanism, “binding-by-synchrony” (BBS), posits that high-frequency oscillations, synchronized between widespread cortical areas, form transient integrated networks of activity across the cortex (1, 2). In this model, rhythmic pulses of depolarization in different cortical locations modulate neuronal firing such that their cells fire in coordinated spatial patterns. Considerable evidence supporting (3) and questioning (4, 5) this hypothesis has been obtained, but studies have been mainly confined to the visual system of rodents and cats, and whether it is tenable in the human neocortex is unclear.

In a seemingly unrelated stream of research, high-frequency oscillations (“ripples”) in the rodent hippocampus during non-rapid eye movement (NREM) sleep have been shown to organize the firing of cells, replaying those encoding events from previous waking periods, critical for memory consolidation in the cortex (6–9). Ripples also occur in the rodent association cortex, where they couple with hippocampal ripples during sleep following spatial memory tasks (10).

Similar events have recently been found in humans during waking and NREM sleep (11–17). Hippocampal formation and cortical ripple occurrence and co-occurrence increase preceding memory recall (11, 12, 15), and cortical neuron firing sequences established during encoding replay during ripples prior to recall (18) and during resting or NREM sleep when consolidation may occur (19, 20). These findings are consistent with cortical ripples contributing to memory consolidation and recall in humans. Specifically, ripple co-occurrence could facilitate the binding of different elements of memories that are represented in disparate cortical areas, the essence of hippocampus-dependent memory (21).

Recently, we found that ~100-ms-long ~90-Hz ripples are ubiquitous in all regions of the cortex during NREM as well as waking (14). During waking, cortical ripples occur on local high-frequency activity peaks. During sleep, cortical ripples occur, often during spindles, and typically on the down-to-upstate transition, with unit-firing patterns

Significance

The binding (integration) of widespread neural activity across the brain is crucial for cognition. However, the mechanisms that support neural binding are poorly understood. Ripples are bursts of high-frequency oscillatory activity that have recently been shown to synchronize across the cortex and may play a role in coordinating neuronal firing. Here, using microelectrodes implanted in the human brain, we show that the co-occurrence of ripple oscillations in sleep and waking enhances the coupling between neurons separated by up to 16 mm. Ripples facilitate neuronal coupling in a phase-dependent manner and can organize the firing in entire assemblies of neurons. This study provides micro-physiologic evidence that ripples may bind neural activity across separated cortical regions.

Competing interest statement: The Massachusetts General Hospital Translational Research Center has a clinical research support agreement with Neuralink, Paradromics, and Synchro, for which L.R.H. and S.S.C. provide consultative input. E.H. is on the Scientific Advisory Boards of Cortechs.ai and Precision Neurotek. Their products are not used in the current manuscript. The remaining authors declare no competing financial interests.

This article is a PNAS Direct Submission.

Copyright © 2023 the Author(s). Published by PNAS. This open access article is distributed under [Creative Commons Attribution-NonCommercial-NoDerivatives License 4.0 \(CC BY-NC-ND\)](#).

¹To whom correspondence may be addressed. Email: iverzhbi@health.ucsd.edu or ehalgren@health.ucsd.edu.

²S.S.C. and E.H. contributed equally to this work.

This article contains supporting information online at <https://www.pnas.org/lookup/suppl/doi:10.1073/pnas.2312204121/-DCSupplemental>.

Published December 29, 2023.

consistent with generation by pyramidal-interneuron (PY-IN) feedback (14, 22). Ripples co-occur, and remarkably, phase-synchronize across all lobes and between both hemispheres, with little decrement, even at long distances (15).

Ripples' widespread co-occurrence and synchrony suggest they may serve a role in binding neural activity across disparate regions of the brain that is more general than their putative involvement in memory consolidation and recall. Studies of intracranial microelectrodes implanted in humans have shown that cortical ripples modulate local neuronal firing in a phase-dependent manner (12, 14, 23). However, a core prediction of the BBS hypothesis extends beyond local firing and posits that gamma-band synchrony across multiple sites facilitates integration of cortical computations across locations through phase selection of local neural activity (2). This concept proposes that co-occurring high-frequency oscillations comodulate involved neurons, enhancing their pairwise interactions and their impact on downstream circuits. While ripples have been shown to synchronize across cortical locations, the impact of co-rippling on the integration of firing across these areas has not been tested in humans.

Here, we analyzed a rare collection of intracranial Utah Array (UA) recordings with 96 fine-tipped microelectrodes at 400- μ m pitch implanted into cortical supragranular layers II/III, each spanning a ~16-mm² region of the cortex. We include multi-hour recordings from single arrays implanted in the temporal lobe of two patients undergoing evaluation of pharmacoresistant epilepsy, and dual arrays simultaneously implanted in the primary motor cortex of a patient with tetraplegia participating in the BrainGate clinical trial (20, 24). We detected and classified putative PY and IN units along with ripple oscillations in the local field potential (LFP) in NREM sleep and spontaneous waking. We show that co-occurring ripples increase co-firing between cells up to 16 mm apart. Co-ripples organize firing latencies and increase the ability of neurons to predict the activity of other neurons in other cortical locations. The increase in pairwise neural prediction is modulated by the relationship between the unit and ripple phase for neurons in both the target and predicting sites. Finally, we show that the expression of neural assemblies formed by groups of neurons is increased when member neurons are engaged in co-ripples. Together, these results support the fundamental core of the BBS hypothesis, that co-occurring ripple oscillations increase the integration of neuronal firing of neurons in different cortical locations and do so in part through phase-modulation.

Results

Characterization of Units and Ripples in Motor Cortex and Temporal Lobe. We analyzed UA recordings (Fig. 1A) from two patient groups (Fig. 1B). Patients E1 and E2 had arrays implanted on the surface of the anterior temporal gyrus. Clinical electrodes were implanted in these patients for ~7 d to define the margins of the resection planned to treat their medication-resistant focal epilepsy. The clinical team determined prior to implantation that there was a very high probability that the resection would include the location where the UA was placed, and this was indeed the case. Patient B1 suffered from tetraplegia secondary to a cervical spinal cord injury. Two arrays were implanted in the primary motor cortex of patient B1 as part of the BrainGate clinical trial to develop a brain-controlled movement prosthesis (20). The cortex at the electrode sites is thought to be healthy, but the patient did have encephalomalacia in the left inferior frontal lobe. All patients gave their fully informed consent, and all procedures were monitored and approved by the review of Institutional Review Boards at Massachusetts General Hospital

and Providence VA Medical Center. NREM was selected from all arrays (418 ± 248 min) and spontaneous waking was selected from patient E1 (154 min) and the dorsal array in patient B1 (173 min; Table 1 and Fig. 1 F and G). A total of 437 PY and 72 IN were sorted and classified from 254 microelectrode channels (127 ± 65 units per array, Fig. 1 C and D). Ripples were detected during NREM and waking based on previously described methods (14, 15). Per-channel ripple density, amplitude, duration, and frequency were 18.6 ± 6.0 min⁻¹, 14.2 ± 5.3 μ V, 107 ± 19 ms, and 89.3 ± 0.9 Hz during NREM and 12.4 ± 4.7 min⁻¹, 18.6 ± 4.9 μ V, 97 ± 29 ms, and 89.8 ± 0.9 Hz during waking. Ripple characteristics are similar to those previously found (12, 14, 15) and did not substantially differ between seizure patients and the BrainGate patient (SI Appendix, Fig. S2). When a ripple detected on the same microelectrode contact contained a spike, there was an average of 1.63 ± 0.60 PY spikes and 2.08 ± 1.14 IN spikes during the single ripple event in NREM and 1.58 ± 0.47 PY spikes and 1.72 ± 0.86 IN spikes in waking. No comparisons were made between units recorded on the same channel.

Unit Firing Increases during, and Phase Locks to, Ripples in the Motor Cortex and Temporal Lobe. Before testing how co-occurring ripples modulate unit co-firing, we measured how unit firing rates changed during ripples. Spike rates for each unit were quantified in the motor cortex and temporal lobe during ripples detected on the unit's channel and compared to baseline periods, which were randomly selected epochs in between ripples on the same channel. Both PYs and INs increased firing during ripples in the motor cortex and temporal lobe during NREM and waking. The mean \pm SD baseline spike rate for PYs and INs was 1.43 ± 1.81 Hz, and 2.82 ± 3.65 Hz in NREM, and 3.30 ± 2.52 Hz and 4.70 ± 6.52 Hz in waking. During ripples, the spike rates for PYs and INs increased to 4.19 ± 5.25 Hz and 8.46 ± 11.34 Hz in NREM, and 5.76 ± 5.52 Hz and 8.85 ± 11.37 Hz in waking ($p_{PY_NREM} = 7.05e-36$, $p_{IN_NREM} = 3.75e-10$, $p_{PY_wake} = 6.08e-17$, $p_{IN_wake} = 3.22e-6$, one-sample two-sided Wilcoxon signed-rank).

In addition to increasing firing rates during the ripple period, our data (14) and others (12, 23) have shown that firing tends to be modulated by ripple phase (Fig. 1 H and I). We quantified the extent to which the neurons in the data included in this study phase-locked with ripples. In total, 272/437 (62%) PY and 61/72 (85%) IN phase-locked to ripples in NREM, while 147/217 (68%) PY and 35/44 (80%) IN phase-locked to ripples in waking (binomial test of spike ripple phase distributions within $0 \pm \pi/2$ vs. $\pi \pm \pi/2$, expected value = 0.5, false discovery rate (FDR) (25) corrected $P < 0.05$).

Ripples Co-Occur within and across Arrays with Zero Phase Lag. Co-ripple rate (i.e., the percent of ripples on two contacts that overlap by 25 ms or more) was greatest for adjacent contacts in the temporal lobe, falling rapidly and reaching a plateau of 15% at a distance of ~1.5 mm (Fig. 2A). The motor cortex demonstrated slightly higher overall co-ripple rates, reaching a plateau of 20% at a distance of ~2.0 mm (Fig. 2B). The BBS hypothesis posits that high-frequency oscillations not only co-occur, but phase synchronize across disparate brain regions. Therefore, in addition to co-occurrence rate, we evaluated phase synchrony across the array during co-ripples using the phase-locking value (PLV), a measure of phase-lag consistency invariant to amplitude (26). The PLV during co-ripples was elevated across all distances compared to NREM epochs absent of detected ripples (FDR-corrected $\alpha = 0.001$ for 10 distance bins, $P \approx 0$). Similar to co-occurrence rate, PLV decayed to a plateau in the temporal lobe and motor cortex (Fig. 2 C and D).

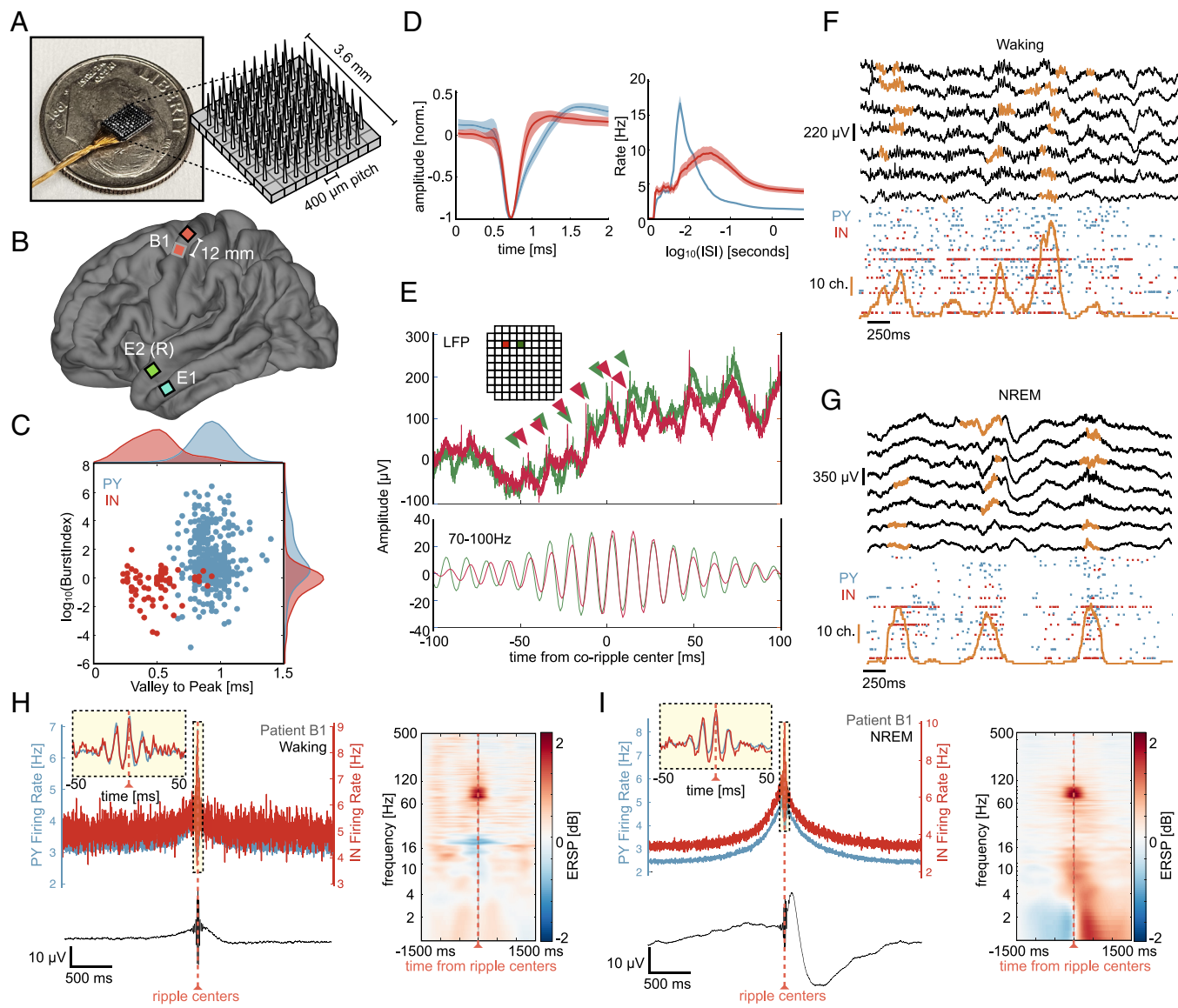


Fig. 1. UA implantation, unit firing during detected ripples. (A) Image of microelectrode configuration across array. (B) Array implantation locations for all patients (2 epilepsy, 1 BrainGate with 2 arrays). (C) Burst index and valley-to-peak time shown for putative PY (blue) and IN (red) units detected across all arrays. (D, Left) mean \pm SD waveforms shown for PY and IN. (Right) mean \pm SEM inter-spike interval (ISI) plots shown for PY and IN. (E, Top) example of broadband 30 kHz LFP data for a co-ripple occurring across two contacts (red and green). Carrots show single unit action potentials occurring on ripple peaks for each contact. (Inset) location of each contact on UA (separated by 0.4 mm). (Bottom) 70 to 100 Hz filtered data showing phase synchrony in the ripple band. (F, Top) sweep of broadband (0.1 to 1,000 Hz) LFP in 7 example microelectrodes during waking with detected ripples in orange. (Bottom) raster plot of associated PY and IN spiking with the number of microelectrodes containing a detected ripple in orange (vertical orange scale bar represents 10 microelectrode channels). (H, Top Left) PY and IN firing rates locked to local ripple centers during waking. (Bottom Left) mean broadband LFP locked to ripple centers. (Right) average time-frequency plots locked to ripple centers detected on an example microelectrode. (G and I) same as in (F and H) but during NREM.

We next examined whether the relatively high level of co-rippling and phase-synchronization in adjacent contacts resulted from local clusters of co-rippling modules. To explore the spatial extent of rippling modules, we employed non-negative matrix factorization (NMF), a location-naïve clustering algorithm. In the temporal lobe, the NMF clusters were in fact spatially contiguous, with cluster sizes of 1.29 ± 0.12 mm (mean \pm SD) during NREM and 1.21 ± 0.09 mm during waking. Clusters were slightly larger in the motor cortex, with cluster sizes of 1.98 ± 0.13 mm during NREM and 2.03 ± 0.19 mm during waking (*SI Appendix*, Fig. S4). These results are consistent with previous attempts to estimate the size of functional modules in the temporal lobe (27). To determine whether ripples exhibited any stereotyped phase lag across the array(s), we computed the pairwise preferred phase between UA microelectrode contacts. The mean \pm SEM

phase lag between contacts during co-ripples was 0.07 ± 0.003 rad during waking and -0.12 ± 0.004 rad during NREM (Fig. 2 E and F). Co-ripple lags were near-zero for all patients, determined using a binomial test of the proportion of preferred co-ripple phase lags in the interval $[-\pi/9, \pi/9]$ against a null proportion of 1/9.

Co-Rippling Increases Unit Co-Firing during Waking and NREM. We next tested the prediction of BBS that co-firing across cortical locations is greater when those locations are co-rippling. Indeed, the occurrence of unit co-firings during co-ripples that overlapped by at least 25 ms was increased compared to duration-matched ripple-absent control periods during NREM (mean \pm SEM: 0.655 ± 0.006 Hz vs. 0.185 ± 0.002 Hz, $P \approx 0$, one-sample two-sided Wilcoxon signed-rank) and during waking (0.909 ± 0.009 Hz vs. 0.479 ± 0.005 Hz, $P \approx 0$) for each patient included in this study

Table 1. Patient demographics, array implantation locations, and unit yield

Array implantation							Units	
Patient	Age	Sex	Reason for implant	Location	NREM duration (min)	Waking duration (min)	Total PY	Total IN
E1	51	F	Epilepsy	Left anterior middle temporal gyrus	340	154	138	29
E2	45	M	Epilepsy	Right anterior superior temporal gyrus	218	N/A	179	16
B1 - dorsal				Dorsal primary motor cortex		173	79	15
B1 - ventral	36	M	Spinal cord injury	Ventral primary motor cortex	695	N/A	41	12

(Fig. 3 A and B). Co-firing was increased for unit pairs spanning all distance bins within arrays for NREM and waking (paired Student's *t* test, FDR-corrected $\alpha = 0.001$ across distance bins). During NREM, the increase in co-firing was maintained for units up to ~ 16 mm apart across both M1 arrays (0.387 ± 0.009 Hz vs. 0.155 ± 0.004 Hz, $P \approx 0$). Within-array co-firing during co-ripple periods increased by 164% for PY↔PY, by 209% for PY↔IN, and by 296% for IN↔IN interactions during waking. In NREM, within-array co-firing increased by 329% for PY↔PY, by 374%

for PY↔IN, and by 430% for IN↔IN interactions. Across M1 arrays, co-firing increased by 241% for PY↔PY, by 254% for PY↔IN, and by 254% for IN↔IN interaction (see SI Appendix, Table S1 for all interaction-specific firing rates).

Unit Co-Firing Increases during Co-Ripples are Not Dependent on Coupling with Upstates, but are Larger when They Do. Given previous reports that ripples tend to couple with slow waves during NREM (10, 14), we quantified how ripple-induced co-firing

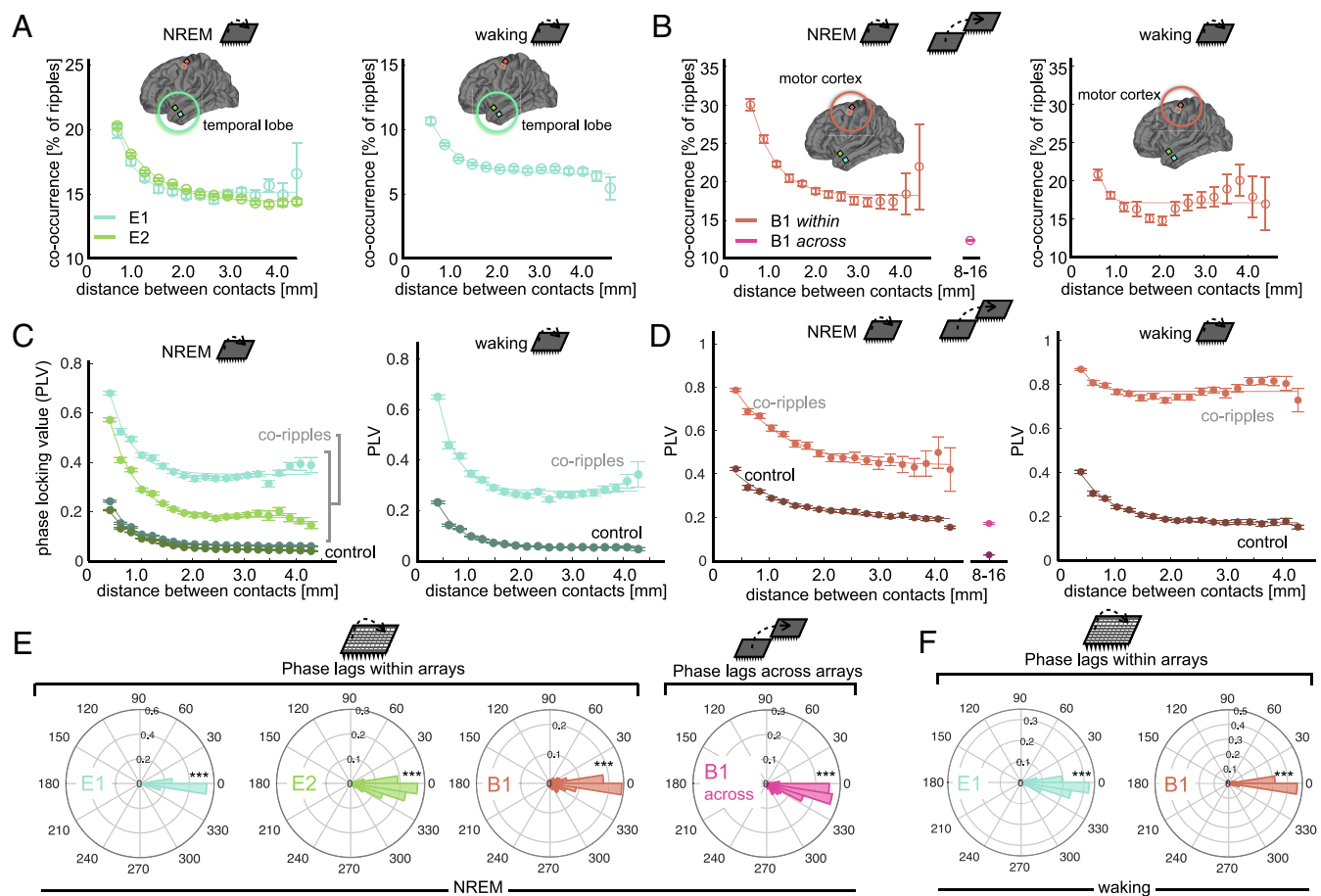


Fig. 2. Ripple co-occurrence and phase locking. (A) Mean \pm SEM ripple co-occurrence rate as a function of distance in the temporal lobe during NREM (Left) and waking (Right). The percent of ripples that overlap by a minimum of 25 ms is shown along the abscissa. (B) Same as A, but for the motor cortex. Ripple co-occurrence is shown across both UA in NREM. (C) PLV during co-ripples over distance during NREM (Left) and waking (Right) in the temporal lobe. PLV for control periods absent of ripples in either channel pair is also shown. Note: PLV does not depend on oscillation amplitude. (D) Same as C but in the motor cortex. PLV is also shown across UA in NREM. (E) Distribution of preferred ripple phase lags within (Left) and across (Right) arrays during NREM. Polar histograms show distribution of circular mean phase lags computed for each channel pair. (F) Same as (E), but during waking. *** $P < 1e-10$ (binomial test of channel pair phase lag distributions within $0 \pm \pi/9$ vs. $\pi \pm 8\pi/9$, expected value = 0.11).

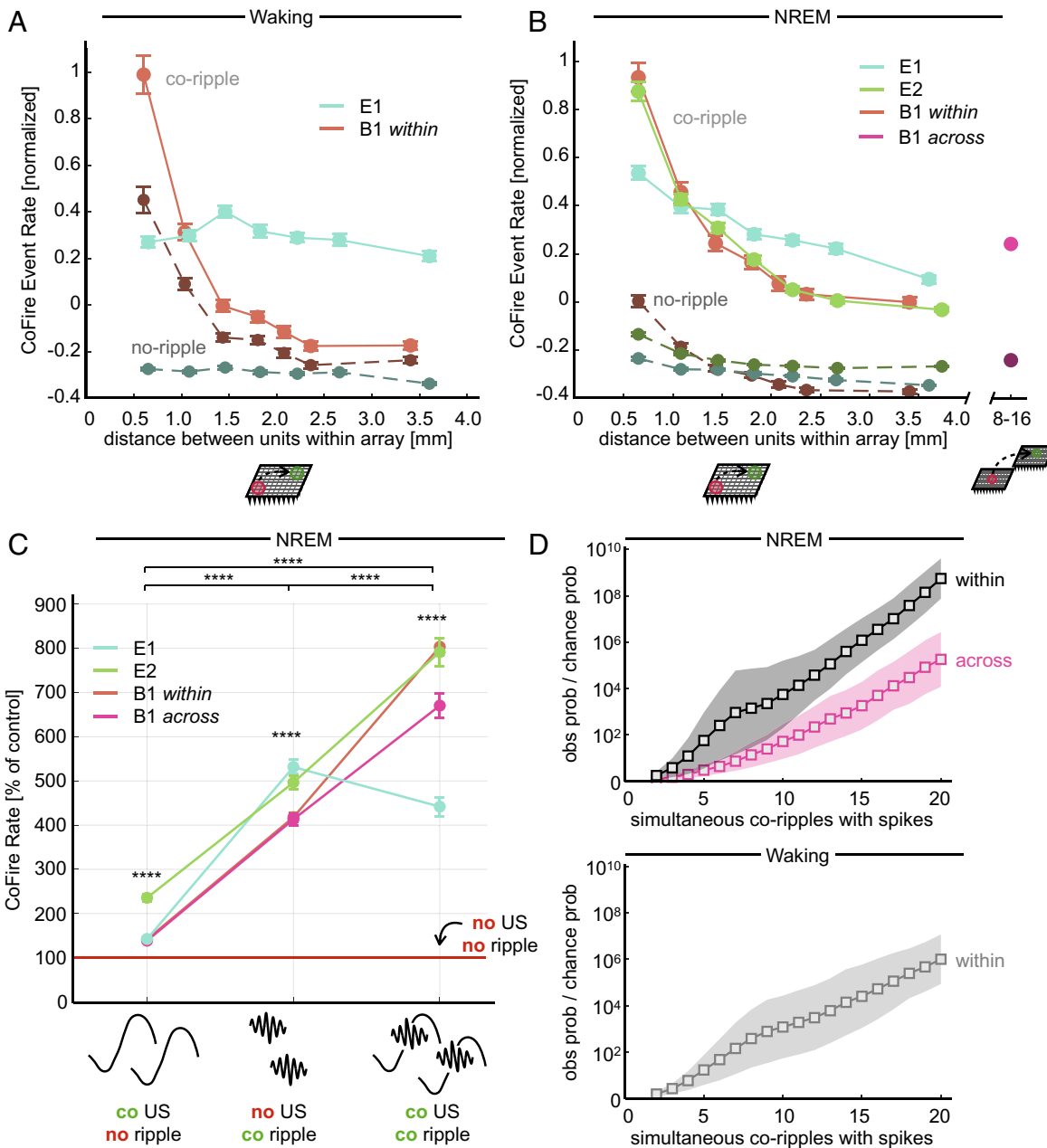


Fig. 3. Co-rippling increases co-firing across sub and supra-millimeter scales. (A) Waking co-firing is increased during co-ripples across entire array. Mean \pm SEM is shown for each distance bin, which each contain an equal number of unit pairs. A co-fire event is defined as a co-ripple period that contains an action potential in both co-rippling sites. Controls are duration-matched periods where neither site is rippling. (B) Same as A, but for co-firing during NREM. All unit pairs that span across both B1 arrays are grouped into the rightmost bin. (C) Co-fire rate within 25 ms across co-occurring upstates without ripples (Left), co-occurring ripples without upstates (Middle), and co-occurring ripples coupled to upstates (Right). Control period is defined as no upstate and ripple in either site ($****P < 0.0001$, one-sample two-sided Wilcoxon signed-rank test). (D) The observed over chance probability that ripples containing at least one spike co-occur increases with the number of spike containing co-ripples. (Top) NREM. (Bottom) waking.

compared with slow-wave-induced co-firing, and whether ripple coupling with upstates influences co-firing (Fig. 3C). We detected upstates during NREM epochs in all electrodes with at least one detected single unit according to previously described techniques (14). Upstates had a mean amplitude and density of $178.3 \pm 63.1 \mu\text{V}$ and $10.1 \pm 2. \text{min}^{-1}$ across UA contacts. Ripples were defined as “coupled” to an upstate if they occurred within a 150-ms window before the upstate peak. Epochs were identified where both ripples and upstates co-occurred on a given electrode pair, where ripples co-occurred without upstates on either electrode, where upstates co-occurred without ripples on either electrode, where neither ripples nor upstates occurred on either electrode

(“baseline”). A co-firing window of 25 ms was used for all analyses in this section, although all results were replicated with a window of 10 ms (SI Appendix, Fig. S5). Co-ripples without upstates increased co-firing by 375% compared to baseline (mean \pm SEM: $1.073 \pm 0.023 \text{ Hz}$, vs. $0.226 \pm 0.006 \text{ Hz}$, $P \approx 0$, one-sample one-sided Wilcoxon signed-rank). In contrast, co-occurring upstates without co-ripples only slightly increased co-firing ($0.332 \pm 0.007 \text{ Hz}$ vs. $0.226 \pm 0.006 \text{ Hz}$, $P \approx 0$). When co-ripples coupled to co-occurring upstates, co-firing was increased an additional 68% compared to isolated co-ripples alone ($1.802 \pm 0.035 \text{ Hz}$ vs. $1.073 \pm 0.023 \text{ Hz}$, $P \approx 0$). Therefore, isolated co-ripples do increase co-firing, and that effect is greater when co-ripples are coupled

to co-upstates. The same ripple/upstate co-firing dynamics were observed between units spanning within and across UA.

Co-Ripples Can Increase Co-Firing beyond that Expected from Increased Overall Firing. If neurons in two locations independently increase their firing rate, the amount of co-firing would also be expected to increase simply due to chance, even if the units are not statistically coupled. We therefore next tested whether the increase in pairwise co-firing during co-ripples is purely a result of the independent increase in firing rates for each unit during their respective ripples. Specifically, we compared the observed co-firing rate during co-ripples to the co-fire rate during a shuffled co-ripple control (i.e., co-ripple periods where the inter-spike intervals (ISIs) for each unit pair are shuffled 1,000 times, $\alpha = 0.05$). Any co-firing above the shuffled control is therefore more organized than what can be explained by the increase in pairwise firing rates alone. For these analyses, we focused on shorter latency unit relationships, and correspondingly defined the co-firing window as 10 ms (roughly the period of a ripple cycle). To exclude very sparsely firing cells, we only examined cell pairs that each had a firing rate of 1 Hz during co-ripple periods between their two sites. For all within-array pairs during waking, 6.70% of PY→PY pairs, 5.01% of PY→IN pairs, and 5.59% of IN→IN pairs showed significantly increased co-firing within 10 ms compared to co-ripple shuffles. During NREM, the proportion of cell pairs exhibiting highly organized firing significantly increased in 6.7% of PY→PY pairs, 6.5% of PY→IN pairs, and 11.2% of IN→IN pairs.

Co-Firing during Co-Ripples Tends to Occur in Multi-Site Groups. We previously found with LFP recordings that the strength of phase-locking between two co-rippling locations strongly increases with the number of additional co-rippling sites. The number of co-rippling sites itself was much greater than expected, and the degree of observed/expected increased exponentially with the number of co-rippling sites (15). Similarly, here we compared the probability of finding spiking in all N sites if those N sites are all co-rippling, to the expected value if co-firing with co-ripples is independent of the number of sites co-rippling (calculated as the product of the probabilities of each of those sites spiking if it is rippling, regardless of whether other sites are rippling). The observed ratio is $\sim 1.4 \times$ higher than expected if $N = 2$, and $\sim 10^8 \times$ higher if $N = 20$ (Fig. 3D). Thus, interaction strength increases rapidly with the number of interacting sites.

Co-Rippling Increases Predictive Firing between Units up to 16 mm apart. The co-firing analysis reported above only considers the co-occurrence of firing within a 25-ms window, without considering the order of spiking, its timing, or a lengthier temporal context. Here, we examine whether the timing of firing by a neuron in one location over an extended period (150 ms) better predicts the firing of another spatially separated neuron when their two locations are co-rippling.

To this end, we predicted the firing of each detected unit by every other simultaneously recorded unit based on a coupling filter constructed from their normalized pre-spike pairwise cross-correlograms (CCG) (*SI Appendix*, Fig. S6). For all prediction analyses, the predicted target neuron is labeled neuron A, while the predicting driver neuron is labeled neuron B. For a given neuron pair, a pre-spike coupling filter between neuron B and neuron A was iteratively constructed, leaving out one action potential in neuron B at a time (mimicking a jackknife bootstrapping technique). The resulting filter was normalized across the pre-spike window such that its sum equaled zero. The removed B spike was fed into the normalized coupling filter, obtaining a B→A

prediction measure for that single spike. Any pair of A and B neurons whose average prediction is greater than zero therefore demonstrated consistently organized firing latencies by neuron B within the window prior to spikes by neuron A. Co-rippling vs no-rippling predictive coupling filters were constructed from equal numbers of spikes for each cell pair to eliminate confounds from increased co-firing during co-ripples (Fig. 4 A and B). As with all co-firing quantification, the coupling between neurons detected on the same contact was not examined in this analysis.

In spontaneous waking, we evaluated prediction for 217 PY, 44 IN, and 36,725 directed cell pairs within UAs implanted in patients E1 and B1. Of all within-array directed cell pairs, 4,261 (12%) had the minimum of 25 B neuron spikes we required for further prediction analyses. Of the cell pairs that met the B spike inclusion criteria, 68% had greater predictive coupling during co-ripples ($P < 1e-10$, paired one-sided Student's *t* test on co-ripple vs. no-ripple prediction). Furthermore, while prediction strength remained near zero across distance bins in non-rippling periods, during co-ripples, it remained significant and above no-ripple levels for unit pairs up to 3.6 mm, the longest distance with enough cell pairs (Fig. 4C). Overall co-ripple prediction was higher than no-ripple controls for all unit type interactions and across all patients in waking (Fig. 4 E and F and *SI Appendix*, Fig. S7). Specifically, prediction during co-ripples was stronger in 66% of PY→PY, 70% of PY→IN, 67% of IN→PY, and 74% of IN→IN pairs that met the B spike count inclusion criterion ($P < 1e-10$, paired one-sided Student's *t* test for all cell type interactions).

In NREM, we evaluated prediction for 437 PY, 72 IN and 73,974 directed cell pairs within UA implanted in all patients. Prediction levels during NREM did not substantially differ from waking levels (Fig. 4D). Out of all possible cell pair combinations in NREM, 9,476 (13%) met B spike inclusion criteria for further analysis. As in waking, overall co-ripple prediction was higher than no-ripple controls for all unit type interactions (Fig. 4 G and H). We found that 76% of PY→PY, 79% of PY→IN, 76% of IN→PY, and 82% of IN→IN pairs were higher during co-ripples ($P < 1e-10$, paired one-sided Student's *t* test for all cell type interactions).

In the dual array separated by 7 to 16 mm, prediction was measured for 120 PY and 27 IN cells during NREM, leading to 4,982 total directed cell pairs and 2,160 (43%) pairs meeting inclusion criteria that spanned across both arrays, compared to 69% within the dorsal array of patient B1. Overall, prediction was comparable across arrays compared to within-array levels in patient B1 (Fig. 4D). Prediction was significantly higher during co-ripples (Fig. 4I) in 68% of PY→PY, 72% of PY→IN, 69% of IN→PY, and 62% of IN→IN pairs ($P = 0.03$ for IN→IN pairs, $P < 1e-10$ for all other cell type interactions, paired one-sided Student's *t* test). Thus, co-ripple facilitation of unit-unit firing prediction is present in both temporal cortex and motor cortex, within and across arrays, as well as in spontaneous waking and NREM.

As an additional control, we also recomputed pairwise prediction when the target region (unit A) had a detected ripple, but the driving region (unit B) did not. Prediction during co-ripples remains higher than the single ripple control at all distances (Fig. 4 B–D), suggesting that it is the co-occurrence of overlapping ripples that encourages unit interaction.

The increased prediction strength during co-rippling vs. no-rippling periods was robust to variations in the parameters used to compute predictive coupling between cells. The difference between co-ripple and no-ripple conditions remained significant across pre-spike coupling filter widths between 50 and 750 ms and pre-filter baseline window lengths from 0 to 600 ms (*SI Appendix*, Fig. S9).

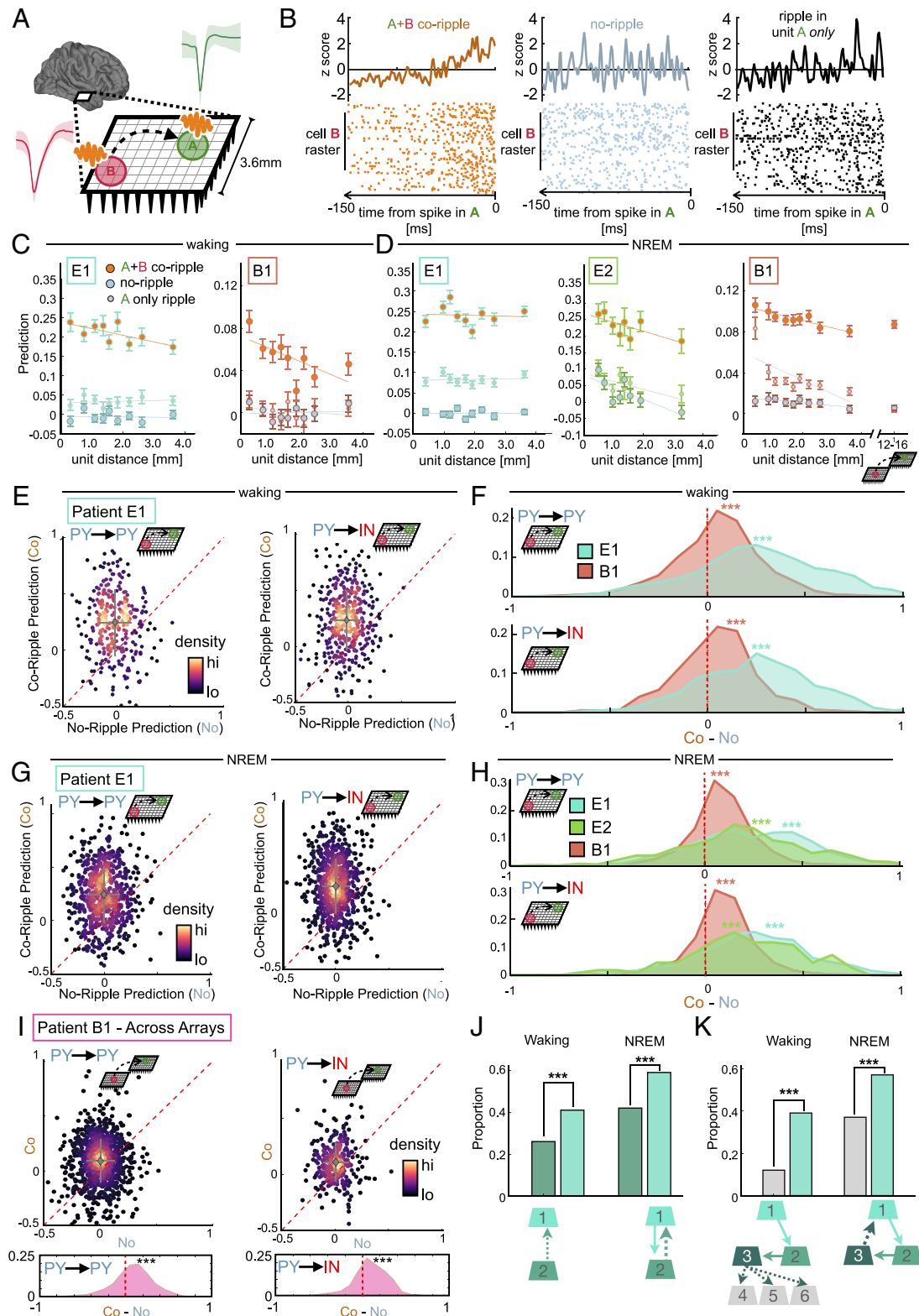


Fig. 4. Co-rippling increases pairwise predictive neural firing patterns. (A) Quantification of predictability: The ability of neural activity of a driver neuron in site B to predict firing of a target neuron in site A when the two sites are co-rippling ("co-ripple") vs. when neither is ("no-ripple") or when only the target site is ("unit A ripple"). (B) Prediction filter design. Cross-correlograms between neurons (A and B) are computed, smoothed and z-scored within a 150-ms window. Relative A-B firing times are fed into the filter, obtaining a prediction value for each action potential in the B neuron. This process is repeated when each site is co-rippling, each site is not rippling, and only the target location is rippling (controlled for the number of B action potentials). (C) Co-ripple, no-ripple, and unit A only ripple prediction during waking within arrays. Mean \pm SEM is shown for distance bins with an equal number of unit pairs. (D) same as C, but during NREM and additionally showing prediction between arrays for patient B1. (E) Scatter plot of mean within-array co-ripple prediction and no-ripple prediction for each unit pair in patient E1 for PY \rightarrow PY and PY \rightarrow IN interactions. Data are shown for waking. The dashed red line is where co-ripple = no-ripple predictability. (F) Histogram of within-array co-ripple minus no-ripple prediction distributions for patients E1 and B1 during waking. (G) Same as E but showing prediction during NREM. (H) same as F but for all patients during NREM. (I) same as G but showing prediction for all unit pairs spanning across arrays in patient B1. (J) Quantifying reciprocal predictive connections. Bar graphs show the probability that cell 2 predicts 1 when cell 1 does predict 2 (light turquoise) and 1 does not predict 2 (dark turquoise). (K) Quantifying reciprocal connections in ordered triplets. The bar graph shows the probability that cell 3 predicts cell 1 (light turquoise) and cell 3 predicts any other cell in the UA (gray) in networks when 1 predicts 2 and 2 predicts 3. *** $p < 1e-4$.

Finally, to examine the effect that increased firing rate had on prediction, we lowered the co-ripple firing rate below no-ripple levels by removing trials from the co-ripple condition until the firing rate was comparable to the control. Equating co-ripple and no-ripple firing rates did not substantially impact the magnitude of co-ripple prediction (*SI Appendix*, Fig. S11).

Unit-Ripple Phase Locking Modulates Predictability. A key tenet of the BBS hypothesis is that the phase of synchronized gamma oscillations modulates neural excitability in different cortical locations at precise timescales, thus facilitating their interactions. We therefore sought to examine whether the consistency between neural firing and LFP oscillation phase during co-ripples influences pairwise predictive coupling. We first quantified how the phase-locking between neural firing and ripple phase correlated with prediction magnitude for pairs of neurons that are significantly coupled during co-ripples (Fig. 5 *A* and *B*). In NREM, the PLV between the driver neuron (PLV_B) and ripple phase was positively correlated with prediction level during co-ripples ($r_B = 0.38$, $P < 1e-10$, Pearson's correlation). The same relationship was true between the PLV of the target neuron (PLV_A) and ripple phase ($r_A = 0.31$, $P < 1e-10$). The strength of correlation was slightly

greater when the PLVs from neurons A and B (PLV_{A+B}) were summed ($r_{A+B} = 0.44$, $P < 1e-10$), suggesting a possible combinatorial effect of phase-locking in both the driving and target regions. Examination of this effect by plotting prediction for different deciles of target and driver PLV (Fig. 5*D*) indicated that prediction is low ($<\sim 0.25$, especially during NREM) unless target and driver PLV are high (>80 th percentiles), in which case prediction is ~ 0.45 .

We tested this finding statistically with bootstrapping analysis of the PLV_A, PLV_B, and PLV_{A+B} correlations. These analyses showed that the summed PLV correlated strongest with prediction ($r_{A+B} - r_A$: 0.13 [0.11–0.16], $r_{A+B} - r_B$: 0.05 [0.04–0.07], median [95% CI], 1,000 iterations). Notably, the subset of neuron pairs that spanned across both arrays in patient B1 exhibited the same PLV-prediction relationships ($r_A = 0.22$, $P < 1e-5$, $r_B = 0.29$, $P < 1e-5$, $r_{A+B} = 0.34$, $P < 1e-5$, $r_{A+B} - r_A$: 0.13 [0.07–0.18], $r_{A+B} - r_B$: 0.05 [0.00–0.10]). During waking, ripple-phase PLV for both the driving ($r_B = 0.42$, $P < 1e-10$) and target ($r_A = 0.36$, $P < 1e-10$) neural activity were also positively correlated with prediction. The correlation was also slightly stronger during waking when the driver and target neuron PLVs were summed ($r_{A+B} = 0.50$, $P < 1e-10$, $r_{A+B} - r_A$: 0.14 [0.11–0.18], $r_{A+B} - r_B$: 0.08 [0.04–0.11]). The PLV relationships with prediction were significant for each

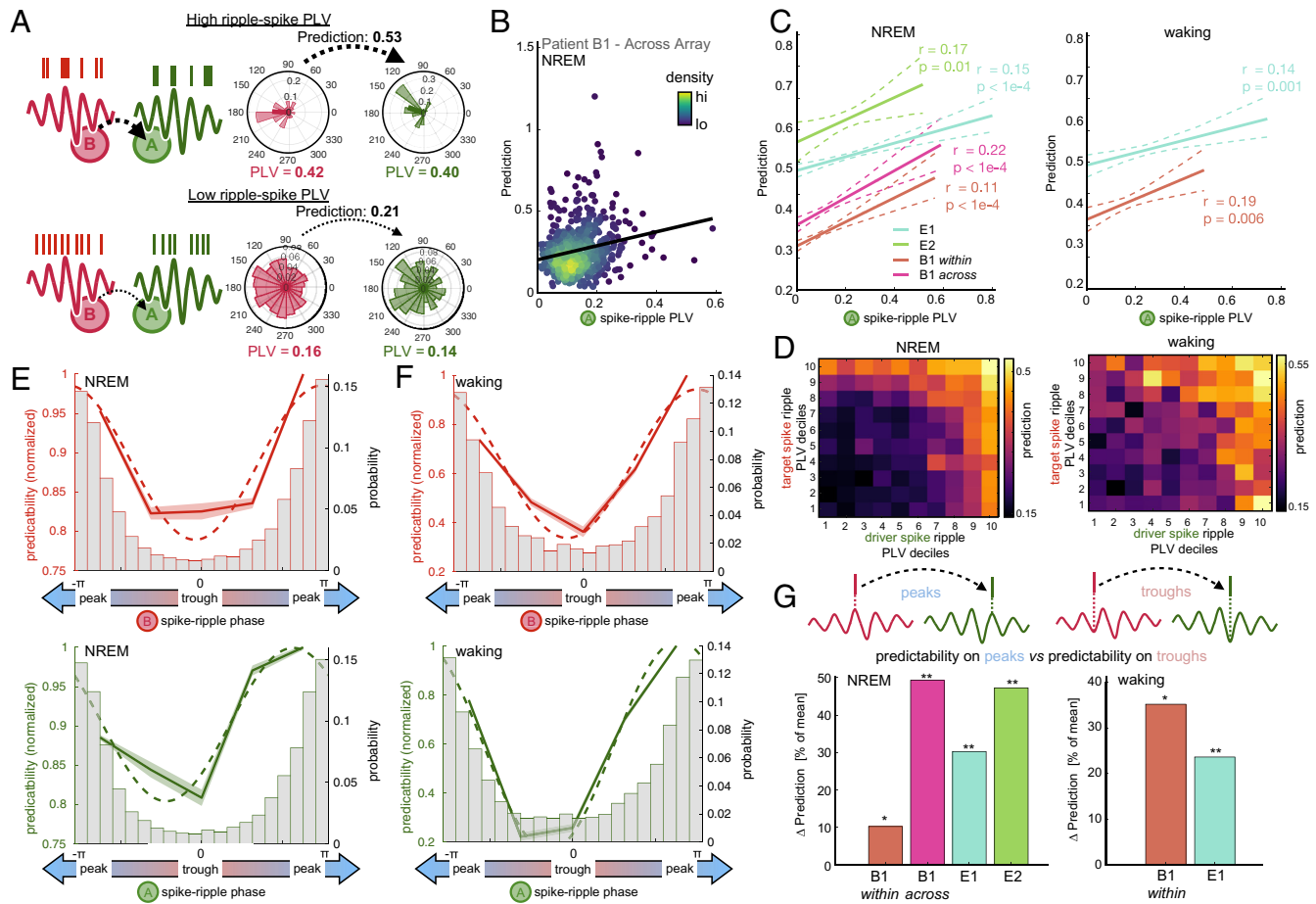


Fig. 5. Spike-phase relationships modulate prediction during co-ripples. (A) Schematic depicting the prediction for a high PLV (Top) and a low PLV (Bottom) neuron in the driving (i.e., B) and target (i.e., A) locations. (B) Co-ripple prediction is positively correlated with the level of phase locking between the A neuron and the ripple. Each dot represents a unit pair that spans across arrays in patient B1 ($N = 560$ pairs, $r = 0.29$, $P < 0.01$). (C) Prediction relationship with A spike-ripple PLV during NREM and (D) during waking. (E) Mean prediction across driver spike and target spike PLV deciles. Prediction is strongest when both the target and driver spikes are highly phase locked to the ripple (Upper Right quadrant). Results are shown for NREM (Left) and waking (Right). (E, Top) prediction as a function of preferred B spike-ripple phase across all subjects. (Bottom) prediction as a function of preferred A spike-ripple phase across all subjects. Normalized mean prediction is shown across all unit pairs for 5 equally spaced bins from $-\pi$ to π . The dashed line shows the best sinusoidal curve fit. Histogram shows the distribution of ripple phase preference for B (Top) and A (Bottom) neurons. (F) Same as E but during waking. (G) Change in prediction when both A and B spikes are on ripple peaks vs. when both are in ripple troughs. For each subject, Δ prediction is computed for all A-B pairs during co-ripples. (Left) NREM. (Right) waking. (* $P < 0.05$, ** $P < 0.01$, one-sided paired Student's *t* test).

individual patient during waking and NREM (Fig. 5C). Together, these results suggest that the consistency between neural spiking and oscillation phase during co-ripples in both the driving and target cells influences the magnitude of their coupling (Fig. 5D).

Of note, we found a significant negative correlation between PLV and firing rate in the driver neuron during waking ($r = -0.40$, $P < 1e-10$) and NREM ($r = -0.29$, $P < 1e-10$). In addition, we found that prediction was also negatively correlated with driver neuron firing rate during waking ($r = -0.50$, $P < 1e-10$) and NREM ($r = -0.39$, $P < 1e-10$). Last, we measured a significant negative correlation between unit firing rate modulation by ripples and the unit's baseline firing rate during waking ($r = -0.26$, $P = 0.005$) and NREM ($r = -0.13$, $P = 4e-5$). Together, this suggests that the increase in co-ripple promotion of predictive coupling in cells with a lower firing rate is mediated by an increased modulation of firing by ripples and a tighter coupling of that firing to the ripple (SI Appendix, Fig. S8).

Prediction is Increased for Spikes Occurring on the Peaks of Ripple Oscillations. To further test the conjecture of the BBS hypothesis that phase modulation promotes neural interactions, we tested whether stronger prediction was associated with a specific phase of the ripple oscillation, and not simply the overall degree of phase-locking. Specifically, we examined whether the precise phase preference (i.e., peak or trough) of the driver and target neurons influences pairwise prediction. Across all cell pairs, we measured the circular mean ripple phase preference and average prediction for both the driver and target neurons during co-ripples. Prediction was significantly sinusoidally modulated by preferred ripple phase in both NREM and waking (sinusoidal fit significance determined from 1,000 shuffled permutations of prediction—phase pairings, SI Appendix, Fig. S10). In both behavioral states and for both driver and predicting neurons, phase preferences around the ripple peak showed higher prediction compared to phase preferences around the ripple trough (Fig. 5E and F). The same modulation of prediction by phase was observed for unit pairs within and spanning across arrays. This indicated that neuron pairs with higher predictive coupling tended to have both driver and target neurons with phase preferences at the peak of the ripple.

To gain further insight into the influence of ripple phase on prediction, we next analyzed the subgroup of neuron pairs that had positive prediction during co-ripples. Within each of the co-ripple modulated cell pairs, we compared the mean prediction in the subset of cases when both driver and target spikes occurred on their respective ripple peaks (double peaks) to the subset of cases when they occurred on their respective ripple troughs (double troughs). Within each co-ripple modulated cell pair, prediction increased by 21% for double peaks compared to double troughs during NREM ($P < 1e-10$, paired one-sided Student's t test, $N_{\text{pairs}} = 7,535$), and 25% during waking ($P = 2e-4$, paired one-sided Student's t test, $N_{\text{pairs}} = 2,014$). Double peaks had greater prediction compared to double troughs for all individual subjects, within and across arrays (Fig. 5G). These results suggest that the ripple peak reflects a more favorable environment for the interaction of cells spanning up to 16 mm apart.

Co-Prediction is Enriched for Reciprocal Connections. The above analyses of prediction of firing by one cell by another during co-ripples in their sites were all focused on directed pairs of neurons. We also tested if neurons were mutually predictive. This direct return, where both $1 \rightarrow 2$ and $2 \rightarrow 1$ significantly predict each other's firing during co-ripples represents second-order recurrent activation (Fig. 4J). In NREM, for all significantly predictive $1 \rightarrow 2$ cell pairs, 59% of the reciprocal $2 \rightarrow 1$ connections were predictive, compared

to 42% when $1 \rightarrow 2$ was not significantly predictive ($P < 1e-10$, $X^2 = 119.0$, $df = 1$). In waking, for all predictive $1 \rightarrow 2$ cell pairs, 41% of the reciprocal $2 \rightarrow 1$ connections were predictive, compared to 26% of $1 \rightarrow 2$ pairs that were not significantly predictive ($P = 5e-10$, $X^2 = 38.7$, $df = 1$).

As noted above (Fig. 3D), co-rippling typically engaged more than 2 sites. We thus explored whether recursive co-prediction networks extended beyond two cells by examining prediction across ordered triplets of neurons (Fig. 4K). Given a network where $1 \rightarrow 2$ and $2 \rightarrow 3$ are significantly predictive, we asked what the probability was that 3 significantly predicted the firing of 1 ($3 \rightarrow 1$) vs any other cell in the array ($3 \rightarrow [4,5,6 \dots]$). In NREM, the recursive $3 \rightarrow 1$ connection was predictive in 57% of cases, while 37% of $3 \rightarrow [4,5,6 \dots]$ connections were predictive ($P \sim 0$, $X^2 = 19912$, $df = 1$). In waking, the $3 \rightarrow 1$ connection was predictive in 39% of cases, while the $3 \rightarrow [4,5,6 \dots]$ was predictive in 12% of cases ($P \sim 0$, $X^2 = 7402.3$, $df = 1$). Thus, it appears that ordered sets of neurons where the activity in one predicts the other during co-rippling concatenate and often form recurrent networks of prediction, at least on the scale of a UA.

Co-Rippling Modulates the Expression of Neuronal Assemblies. Neural coding is unlikely to be fully explained by pairwise interactions alone. Recent work in humans (28) suggested that groups of neurons that have significant co-firing tendencies can be categorized into cell assemblies whose expression is linked to episodic memory performance. We next evaluated whether integrated neural assemblies were detectable in our data and whether co-rippling across multiple electrodes facilitates their expression. We detected cell assemblies during NREM and waking according to previously described methods (28, 29). We divided neural spike trains from NREM and waking into 100 ms bins (roughly the duration of a ripple event) and normalized the binned firing rates for each neuron across the recording session. Using a combination of principal component analysis followed by independent component analysis (ICA), we identified groups of neurons with significant coactivation patterns. This produced an array of component weights across all neurons for each assembly, indicating how strongly a neuron contributed to the expression of a given assembly. Highly contributing cells were identified as key member neurons of the assembly if their ICA weight exceeded 1.5 SD above the mean weight (Fig. 6A). The expression of each assembly can be determined by projecting the binned z-scored firing matrix onto the assembly weight vector. We defined assembly activation events when expression exceeded the 95th percentile across the recording (Fig. 6B).

We identified 76 total assemblies during NREM and 40 total assemblies during waking (23 ± 4 per patient per behavioral state). Each assembly had a mean \pm SD of 7.9 ± 3.2 member neurons during waking and 10.6 ± 2.1 member neurons during NREM. Of note, in patient B1 during NREM (when data were available for both UA), key member neurons often spanned across dorsal and ventral arrays (Fig. 6A and B). We compared the mean expression strength during periods when at least one member neuron channel was rippling to periods when no member neuron channels had a detected ripple, but at least one non-member neuron channel did. Mean assembly strength was higher during member rippling periods compared to non-member ripple controls (Fig. 6C) during waking (24% increase, $P = 1e-4$, one-sided paired Student's t test) and NREM (59% increase, $P = 5e-6$, one-sided paired Student's t test). This suggests that precise co-ripple networks, and not generic ripple activation across the array, are associated with the selection of co-active cells. We next measured the activation rate of each assembly as a function of the percent of member

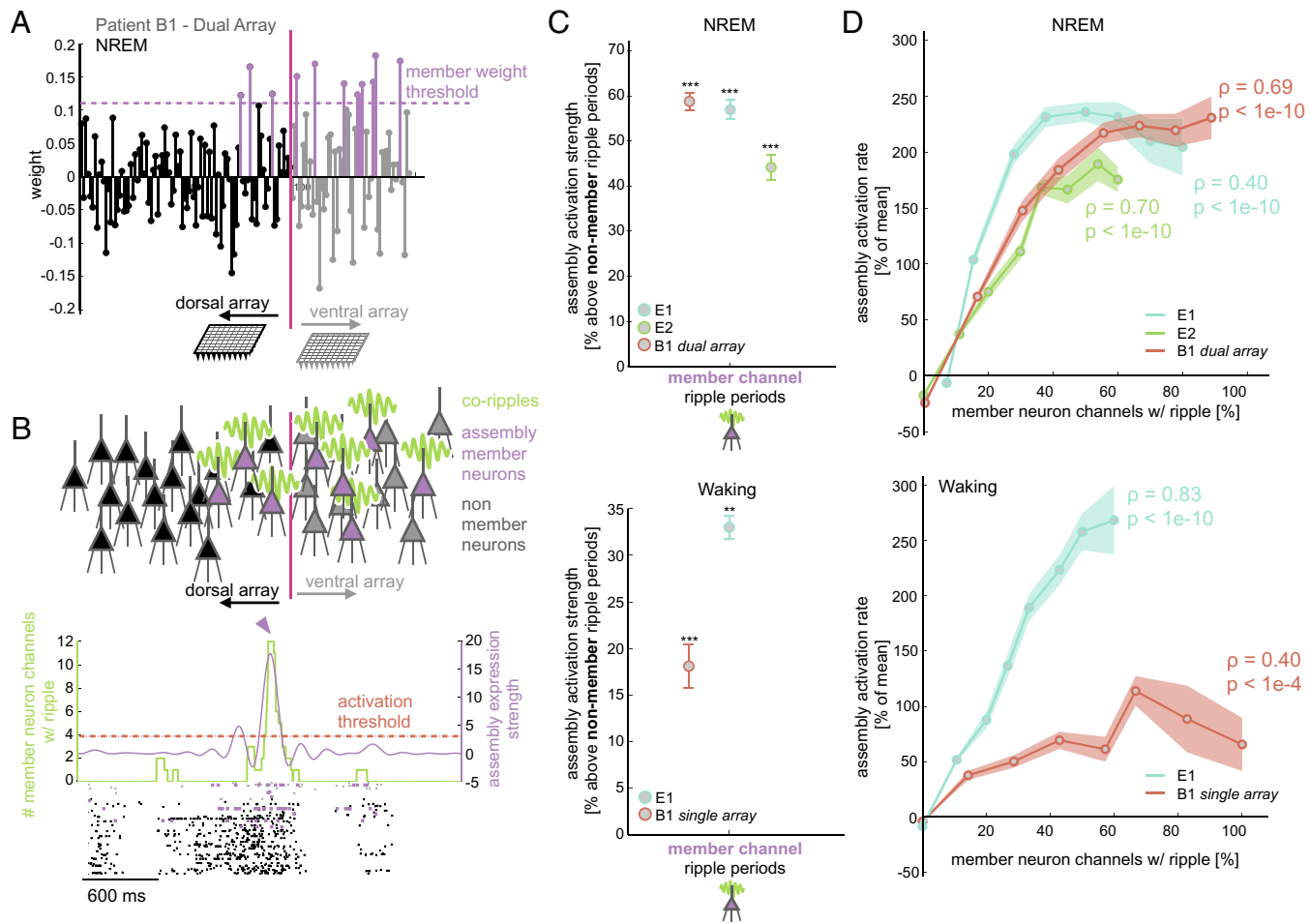


Fig. 6. Co-ripples facilitate expression of neuronal assemblies. (A) Example assembly with identified member neurons that span across both arrays in subject B1 during NREM. (B, Top) schematic depicting assembly member neurons in sites that are co-rippling. (Bottom) example of activation of the assembly in A when all member neuron sites have a detected ripple. Assembly strength (purple curve) and ripple count (green curve) are superimposed on the spike raster of both arrays in subject B1. Colored spike raster depicts cells that were labeled as assembly members. The horizontal dashed red line displays the 95%ile activation threshold, and the purple arrow marks the time where the displayed assembly is activated. The control is defined as periods where member neuron channels have a detected ripple. The control is shown on the Top and waking on the Bottom. (C) Mean \pm SEM assembly strength above control during periods where member neuron channels have a detected ripple. NREM is shown on the Top and waking on the Bottom. (D) Mean (circle marks) \pm SEM (shaded region) assembly activation rate as a function of the proportion of member neuron electrodes that contain a detected ripple. (Top) results in NREM for all patients (Spearman rho = 0.59, $P < 1e-10$). (Bottom) results in waking using data from the medial array in patient B1 and the array in E1 (Spearman rho = 0.50, $P < 1e-10$). The Spearman rho values are displayed for each individual patient. Some traces do not reach 100% since the periods of the recording that contained exactly that number of co-rippling channels were below the minimum duration threshold for analysis (1 s). ** $P < 0.01$, *** $P < 0.001$ one-sided one-sample Student's t test.

neuron channels that were co-rippling. Assembly activation rate was positively and monotonically correlated with the proportion of member neuron channels that were engaged in a co-ripple in NREM ($P = 1e-10$, Spearman rho = 0.57) and in waking ($P < 1e-10$, Spearman rho = 0.52) for all patients (Fig. 6D).

Discussion

The mechanisms by which the cortex binds the activity of neurons in separated locations remain largely unknown. Bursts of high-frequency oscillations ('ripples') have recently been shown to possess some of the characteristics necessary for a role in cortical neural binding (14, 15, 23). They are ubiquitous and consistent in frequency and duration across cortical areas and across waking and sleep. They have a strong tendency to co-occur and phase-lock even at long distances and phase-modulate firing of local PY and IN. While these properties are prerequisites for BBS, they do not establish that the basic function of binding, integration of cortical activity, is facilitated by co-rippling. Such was the goal of the current study.

LFPs and single units were recorded during NREM sleep and waking with four 96-channel microarrays, each implanted in a 16-mm² patch of the human supragranular cortex. Single arrays were implanted in the lateral temporal neocortex of two epileptic patients, and two arrays separated by ~12 mm were implanted in the precentral gyrus of a tetraplegic patient. Across patients, cortical areas, and states, we found increased integration of neuronal firing in different cortical locations when those locations co-ripped, using three measures: co-firing, co-prediction, and assembly expression. These measures of the interaction between the firing of cells across locations differ in their sensitivity to increasing complexity and duration of the predicting spike train. Co-firing only requires that cells fire within 25 ms of each other; co-prediction is sensitive to the temporal structure of firing increases and decreases by the predicting cell in the 150 ms prior to the predicted cell's action-potential; assembly expression detects participation in an extended network involving multiple cells. The similar results obtained with all three measures across areas and states suggest that increased interaction of cortical neuronal firing during co-ripples is a robust phenomenon.

The central mechanism posited to underlie BBS is the synchronous modulation of cell excitability in different locations, whereby action-potentials triggered by depolarization in one location would be effective at triggering action-potentials in another because of its depolarized state (2). This would result in co-firing, and more generally in the selection of neural networks that engage the particular locations that are co-rippling. Accordingly, we found that co-ripples frequently occur within and between UAs, where neurons often fired in phase with the local ripple (15). Critically, we found that the level of this phase-locking is correlated with the ability of neuronal firing in one location to predict the firing in another location. Specifically, prediction is enhanced when both predicting and predicted spikes occur on the ripple peak, as posited by BBS.

Increased co-prediction between units in co-rippling sites is unlikely to reflect a monosynaptic connection because increased co-prediction occurs at long distances without decrement, while monosynaptic connections are rare (~1% at the shortest distance, 400 μm) and decrease with distance (30, 31). However, multi-synaptic connections are possible due to the high fan-out/fan-in of supragranular PY cells. If conduction occurs in the 11 ms between ripple peaks in Driver and Target sites, then there could be three relays: the total transmission time between supragranular pyramids is ~2 ms, including synaptic transmission and spike initiation latency (30) leaving 5 ms for axonal conduction, or 5 mm at 1 m/s. Multi-synaptic connections are also consistent with the long latency range of predictive firing and could be facilitated by the fact that co-ripples typically co-occur in ~6 to 8 sites. Thus, co-ripples facilitate a neuronal network, recursive and reciprocal, visible in the dependence of network activation on the proportion of participating sites with co-ripples. In the absence of ripples, prediction of firing across sites is at chance. Thus, multi-site co-rippling could select a distributed network of co-firing neurons across tens of milliseconds by organizing firing lags that are multiples of the ripple cycle duration.

Some have suggested that ripples do not actively facilitate trans-cortical integration but are simply a byproduct of nonspecific activation (4, 5). However, co-rippling still enhanced co-firing when compared to co-firing to the same spikes with their ISIs shuffled, indicating that the precise relative timing of the spikes in the two locations is critical. Similarly, our method of cross-location prediction balanced the firing in no-rippling and co-rippling predictors, but still found increased prediction during co-rippling. These controls, and the strong effects of phase on prediction, demonstrate that the effects of co-ripples extend beyond those due to co-activation.

The arrival of an action-potential from one location to another not only has a higher probability of evoking a spike in the post-synaptic cell if it arrives on the depolarized ripple phase, it also augments that depolarization, and thus contributes to the ripple. Furthermore, we found that co-ripple-enhanced prediction is reciprocal (if neuron 1 predicts 2 then 2 likely predicts 1) and recurrent (if 1 predicts 2 which predicts 3, then 3 likely predicts 1). Thus, co-ripples could initiate positive feedback loops that sustain and possibly augment specific patterns. These considerations suggest that a strongly positive relationship may be found between increasing levels of co-rippling and measures of firing interaction. Indeed, we found a large increase in co-firing during co-ripples with increasing co-rippling and co-firing in other sites. Similarly, the level of assembly activation increases steeply with an increasing proportion of sites that are co-rippling. Thus, increased firing and phase modulation may be better viewed as synergistic and mutually reinforcing rather than as alternatives.

Most previous studies of ripples were of hippocampal ripples in rodents during NREM sleep where they play a critical role in facilitating cortical consolidation, in conjunction with slower waves including cortical upstates (7, 8). We previously found that cortical ripples in humans are strongly related to upstates during NREM (14). Here, we found that the co-occurrence of either upstates or ripples alone increases co-firing, with the increase due to co-ripples about twice that due to co-upstates. However, when both co-upstates and co-ripples occur together, the increase in co-firing is much greater than either alone. The window for these increases is 25 ms, the window when spike timing-dependent plasticity modulates synaptic strength (32). Thus, these results reinforce the potential role of nested oscillations in promoting consolidation during sleep.

There are several limitations to this study. First, data are provided from only three patients, two of whom have long-standing epilepsy. However, no interictal spikes or seizures were observed in the epochs studied here, and no pathology was visible in this location in neuroimaging. Critically, ripple characteristics, co-occurrence, and modulation of neural activity were similar between these two patients with epilepsy and the third patient who is paralyzed but has a healthy motor cortex. This work quantifies ripples with intracranial recordings in the healthy human cortex and provides strong evidence that ripples are not epileptic phenomena.

The second limitation is anatomical: We only recorded from supragranular layers of limited regions in two cortical areas. Multi-patch recordings in humans (30) and anatomical studies in primates (33) suggest that horizontal connections may be more intense in layers 2/3, raising the possibility that integrative processes may be different in other layers. Each UA subtends ~16 mm^2 of cortical surface, ~0.007% of the total, and even in the patient with dual arrays the longest distance separating neurons is ~16 mm, ~7% of the longest cortico-cortical streamline distance estimated from Diffusion Tensor Imaging (34). Thus, it is important to confirm our results in larger and more distributed datasets. However, we would note that the effects we describe decrease minimally or not at all over the distances we sampled, and in previous work, the probability of co-rippling and level of phase-locking was largely maintained for over 16 cm (15). Also in relation to this prior work, we demonstrate that the near-zero phase lag between co-ripples observed across the entire brain persists at the micro-physiologic scale as well.

The third limitation is the lack of a behavioral task. While binding of course occurs during spontaneous mentation, and ripples have important putative functions during sleep, this limitation, together with the lack of recordings from the early visual cortex (for clinical reasons), as well as species differences, renders it difficult for us to compare our results directly to most experimental literature testing BBS, which are typically in visual tasks with recordings from early visual cortices in cats or rodents.

In summary, we provide evidence that co-rippling in different cortical locations enhances the integration of their constituent neuronal firing. This finding was replicated with co-firing, co-prediction, and neural assembly activation, in three subjects, two cortical areas, and sleep and waking, for putative PY and INs. When two cortical locations co-ripple, we find a corresponding increase in pairwise neural co-firing and prediction for units detected in those two locations. Co-ripple facilitated prediction is strongly modulated by ripple phase, persists at the longest separations sampled (16 mm), and remains when firing rate increases during ripples are controlled for. These results support in humans key predictions of the BBS model: that ripples co-occurring in different cortical locations facilitate the integration of their neuronal firing through a mechanism involving phase modulation.

Data, Materials, and Software Availability. Anonymized code has been deposited on github (<https://github.com/iverzh/coripple-prediction>)⁽³⁵⁾ and processed data have been deposited in Zenodo (<https://zenodo.org/records/10183659>)⁽³⁶⁾.

ACKNOWLEDGMENTS. We thank Eran Mukamel, Mikio Aoi, Charles Dickey, Adam Niese, Dan Soper, Christopher Gonzalez, and Jacob Garrett for their support. This work was supported by NIMH (RF1MH117155), NINDS (R01NS109553, R25NS065743, UH2NS095548, U01DC017844), American Academy of Neurology Clinical Research Training Scholarship, Harvard Catalyst KL2/CMeRIT (D.B.R.), Department of Veterans Affairs (N2864C, A2295R), Conquer Paralysis Now 004698, Massachusetts General Hospital-Deane Institute (L.R.H.).

Author affiliations: ^aNeurosciences Graduate Program, University of California San Diego, La Jolla, CA 92093; ^bMedical Scientist Training Program, University of California San Diego, La Jolla, CA 92093; ^cDepartment of Neurology, Center for Neurotechnology and Neurorecovery, Massachusetts General Hospital, Boston, MA 02114; ^dDepartment of Radiology, University of California San Diego, La Jolla, CA 92093; ^eDepartment of Neurosciences, University of California San Diego, La Jolla, CA 92093; ^fDepartment of Neurosurgery, Massachusetts General Hospital, Boston, MA 02114; ^gCenter for Neurorestoration and Neurotechnology, Department of Veterans Affairs, Providence, RI 02908; and ^hCarney Institute for Brain Science and School of Engineering, Brown University, Providence, RI 02912

Author contributions: I.A.V., S.S.C., and E.H. designed research; I.A.V., D.B.R., S.K., J.N.K., A.K., Z.M.W., and L.R.H. performed research; I.A.V. contributed new reagents/analytic tools; I.A.V., S.K., and Y.B. analyzed data; and I.A.V., S.S.C., and E.H. wrote the paper.

1. C. von der Malsburg, The what and why of binding: The modeler's perspective. *Neuron* **24**, 111–125 (1999).
2. P. Fries, Neuronal gamma-band synchronization as a fundamental process in cortical computation. *Annu. Rev. Neurosci.* **32**, 209–224 (2009). 10.1146/annurev.neuro.051508.135603.
3. W. Singer, Recurrent dynamics in the cerebral cortex: Integration of sensory evidence with stored knowledge. *Proc. Natl. Acad. Sci. U.S.A.* **118**, e2101043118 (2021).
4. B. Merker, Cortical gamma oscillations: The functional key is activation, not cognition. *Neurosci. Biobehav. Rev.* **37**, 401–417 (2013).
5. P. R. Roelfsema, Solving the binding problem: Assemblies form when neurons enhance their firing rate—they don't need to oscillate or synchronize. *Neuron* **111**, 1003–1019 (2023). 10.1016/j.neuron.2023.03.016.
6. M. A. Wilson, B. L. McNaughton, Reactivation of hippocampal ensemble memories during sleep. *Science* **265**, 676–679 (1994).
7. G. Buzsaki, Hippocampal sharp wave-ripple: A cognitive biomarker for episodic memory and planning. *Hippocampus* **25**, 1073–1188 (2015). 10.1002/hipo.22488.
8. N. Maingret, G. Girardeau, R. Todorova, M. Goutierre, M. Zugaro, Hippocampo-cortical coupling mediates memory consolidation during sleep. *Nat. Neurosci.* **19**, 959–964 (2016). 10.1038/nn.4304.
9. V. Ego-Stengel, M. A. Wilson, Disruption of ripple-associated hippocampal activity during rest impairs spatial learning in the rat. *Hippocampus* **20**, 1–10 (2009). 10.1002/hipo.20707.
10. D. Khodagholy, J. N. Gelinas, G. Buzsaki, Learning-enhanced coupling between ripple oscillations in association cortices and hippocampus. *Science* **358**, 369–372 (2017). 10.1126/science.aan6203.
11. Y. Norman *et al.*, Hippocampal sharp-wave ripples linked to visual episodic recollection in humans. *Science* **365**, eaax1030 (2019).
12. A. P. Vaz, S. K. Inati, N. Brunel, K. A. Zaghloul, Coupled ripple oscillations between the medial temporal lobe and neocortex retrieve human memory. *Science* **363**, 975–978 (2019).
13. B. P. Staresina *et al.*, Hierarchical nesting of slow oscillations, spindles and ripples in the human hippocampus during sleep. *Nat. Neurosci.* **18**, 1679–1686 (2015). 10.1038/nn.4119.
14. C. W. Dickey *et al.*, Cortical ripples during NREM sleep and waking in humans. *J. Neurosci.* **42**, 7931–7946 (2022). 10.1523/jneurosci.0742-22.2022.
15. C. W. Dickey *et al.*, Widespread ripples synchronize human cortical activity during sleep, waking, and memory recall. *Proc. Natl. Acad. Sci. U.S.A.* **119**, e2107797119 (2022). 10.1073/pnas.2107797119.
16. X. Jiang, J. Gonzalez-Martinez, E. Halgren, Coordination of human hippocampal sharpwave-ripples during NREM sleep with cortical theta bursts, spindles, downstates and upstates. *J. Neurosci.* **39**, 8716–8744 (2019). 10.1523/jneurosci.2857–18.2019.
17. X. Jiang, J. Gonzalez-Martinez, E. Halgren, Posterior hippocampal spindle-ripples co-occur with neocortical theta-bursts and down-upstates, and phase-lock with parietal spindles during NREM sleep in humans. *J. Neurosci.* **39**, 8949–8968 (2019). 10.1101/702936.
18. A. P. Vaz, J. H. Wittig, S. K. Inati, K. A. Zaghloul, Replay of cortical spiking sequences during human memory retrieval. *Science* **367**, 1131–1134 (2020).
19. J.-B. Eichenlaub *et al.*, Reactivation of motor-related gamma activity in human NREM sleep. *Front. Neurosci.* **14**, 449 (2020).
20. D. B. Rubin *et al.*, Learned motor patterns are replayed in human motor cortex during sleep. *J. Neurosci.* **42**, 5007–5020 (2022). 10.1523/jneurosci.2074–21.2022.
21. L. R. Squire, Memory and the hippocampus: A synthesis from findings with rats, monkeys and humans. *Psychol. Rev.* **99**, 195–231 (1992).
22. E. Stark *et al.*, Pyramidal cell-interneuron interactions underlie hippocampal ripple oscillations. *Neuron* **83**, 467–480 (2014). 10.1016/j.neuron.2014.06.023.
23. A. P. S. Tong, A. P. Vaz, J. H. Wittig, S. K. Inati, K. A. Zaghloul, Ripples reflect a spectrum of synchronous spiking activity in human anterior temporal lobe. *Elife* **10**, e68401 (2021).
24. J. D. Simen *et al.*, Home use of a percutaneous wireless intracortical brain-computer interface by individuals with tetraplegia. *IEEE Trans. Biomed. Eng.* **68**, 2313–2325 (2021).
25. Y. Benjamini, Y. Hochberg, Controlling the false discovery rate: A practical and powerful approach to multiple testing. *J. R. Stat. Soc. Ser. B (Methodol.)* **57**, 289–300 (1995).
26. J. P. Lachaux, E. Rodriguez, J. Martinerie, F. J. Varela, Measuring phase synchrony in brain signals. *Hum. Brain Mapp.* **8**, 194–208 (1999).
27. J. I. Chaperon, J. H. Wittig, S. K. Inati, K. A. Zaghloul, Micro-scale functional modules in the human temporal lobe. *Nat. Commun.* **13**, 1–14 (2022).
28. G. Umbach, R. Tan, J. Jacobs, B. E. Pfeiffer, B. Lega, Flexibility of functional neuronal assemblies supports human memory. *Nat. Commun.* **13**, 6162 (2022). 10.1038/s41467-022-33587-0.
29. V. Lopes-dos-Santos, S. Ribeiro, A. B. L. Tort, Detecting cell assemblies in large neuronal populations. *J. Neurosci. Methods* **220**, 149–166 (2013). 10.1016/j.jneumeth.2013.04.010.
30. L. Campagnola *et al.*, Local connectivity and synaptic dynamics in mouse and human neocortex. *Science* **375**, eabj5861 (2022).
31. H. Planert *et al.*, Cellular and synaptic diversity of layer 2–3 pyramidal neurons in human individuals. *bioRxiv [Preprint]* (2023). <https://doi.org/10.1101/2021.11.08.467668>.
32. D. E. Feldman, The spike-timing dependence of plasticity. *Neuron* **75**, 556–571 (2012).
33. M. F. Kritzer, P. S. Goldman-Rakic, Intrinsic circuit organization of the major layers and sublayers of the dorsolateral prefrontal cortex in the rhesus monkey. *J. Comp. Neurol.* **359**, 131–143 (1995).
34. B. Q. Rosen, E. Halgren, A whole-cortex probabilistic diffusion tractography connectome. *eNeuro* **8**, ENEURO.0416–0420.2020 (2021). 10.1523/eneuro.0416–20.2020.
35. I. A. Verzhbinsky, coripple-prediction. GitHub. <https://github.com/iverzh/coripple-prediction>. Deposited 22 November 2023.
36. I. Verzhbinsky, *et al.*, Co-occurring ripple oscillations facilitate neuronal interactions between cortical locations in humans. Zenodo. <https://zenodo.org/records/10183659>. Deposited 22 November 2023.